Journal of Alloys and Compounds 650 (2015) 896–906

Contents lists available at ScienceDirect

Journal of Alloys and Compounds

journal homepage: http://www.elsevier.com/locate/jalcom

Effect of Eu addition on the microstructures and mechanical properties of A356 aluminum alloys

Feng Mao [a], Guangyuan Yan [a], Zhenjing Xuan [a], Zhiqiang Cao [b, *], Tongmin Wang [a, **]

[a] Key Laboratory of Materials Modification by Laser, Ion, and Electron Beams (Ministry of Education), School of Materials Science and Engineering, Dalian University of Technology, Dalian 116024, PR China
[b] Laboratory of Special Processing of Raw Materials, Dalian University of Technology, Dalian 116024, PR China

ARTICLE INFO

Article history:
Received 29 May 2015
Received in revised form
27 June 2015
Accepted 29 June 2015
Available online 12 August 2015

Keywords:
Eutectic silicon
Eu modification
A356
Mechanical properties

ABSTRACT

The effect of Eu additions (0, 0.02, 0.04, 0.06, 0.08 and 0.1 wt.%) and T6 heat treatment on the microstructures and mechanical properties of A356 alloy have been investigated in the present work. Microstructures of the as-cast and T6 heat treated samples were examined by optical microscopy (OM) and scanning electron microscopy (SEM). It was found that 0.1%Eu modified the eutectic Si from a coarse plate-like form to a fully modified and fine fibrous one with a better uniform distribution. T6 treatment encouraged the spheroidization of eutectic Si particles. Correlating with the as-cast samples, the 0.1%Eu modified A356 alloy achieved likewise full modification of eutectic Si particles with lowest mean area and aspect ratio. In addition, the coarse and small Eu-rich intermetallics were both found in the 0.1%Eu modified A356 alloy. The cooling curves of A356 alloys showed that increasing Eu addition resulted in increasing nucleation undercooling and increasing growth undercooling. However, the recalescence ($T_G - T_{Min}$) increased by the initial addition of Eu, while it remained relatively stable for increasing additions (above 0.06%). The quenching experiment indicated that a large number of eutectic grains were located at or close to the tips of the aluminum dendrites with a jagged solid–liquid interface in unmodified alloy, while very few eutectic grains were formed in the interdendritic region with a smooth solid–liquid interface in 0.1%Eu modified alloy. An optimal combination of UTS (265 MPa) and EI (14.7%) of A356 alloy was achieved by the 0.1%Eu addition combined with T6 heat treatment.

1. Introduction

The A356 aluminum alloy has widespread applications especially in the aerospace and automotive industries because of the excellent properties including castability, weldability, corrosion resistance and integrated mechanical properties [1,2]. It is a heat-treatable casting alloy which can be strengthened by precipitation of Mg_2Si after T6 treatment [3,4]. The microstructure of A356 alloy exhibits the primary α-Al and plate-like eutectic Si under normal cooling conditions. The brittleness of eutectic Si is the main reason responsible for the poor properties of Al–Si alloys since the coarse and plate-like eutectic Si lead to premature crack initiation and fracture in tension conditions. In order to achieve good tensile properties, eutectic Si should be modified and heat treated. Modification of the eutectic Si from a coarse plate-like to a fine fibrous structure is normally achieved in three different ways: (1) chemical modification, (2) quench modification [5] and (3) ultrasonic vibration [6] and electromagnetic field [7]. With respect to chemical modification, several elements have been widely used in industry today, i.e., Sr [8], Na [9] and Sb [10]. Compared to these common elements, rare earth not only can modify eutectic Si but also can effectively degas and remove slag with environmentally friendly features. These effects make them become a superior choice for the applications in aluminum foundry. Tsai et al. [11,12] reported that the addition of 1.0 wt% La resulted in a fibrous eutectic Si and the addition of 1.0 wt% Ce resulted in only a small degree of refinement of the plate-like eutectic Si in A356 alloys. However, the tensile strengths were not improved after T6. Xu et al. [13] found that the rare earth Sm affected the secondary dendrite arm spacing (SDAS) of primary α-Al and the plate-like eutectic Si was fully modified into a fine fibrous structure when 0.6 wt% Sm was added into the Al–7Si–0.7 Mg alloy. Consequently a good combination of ultimate tensile strength and elongation was

* Corresponding author.
** Corresponding author.
E-mail addresses: caozq@dlut.edu.cn (Z. Cao), tmwang@dlut.edu.cn (T. Wang).

http://dx.doi.org/10.1016/j.jallcom.2015.06.266
0925-8388/

obtained. Li et al. [14] investigated the effects of Y additions on the microstructure of Al–7Si-0.5 Mg alloy. It was found that 0.3 wt% Y modified the eutectic Si from plate-like to fine branched and consequently resulted in the notable improvement of tensile properties. Results obtained in Muhammad's et al. [15] research indicated that with the increase of Sc contents up to 0.4 wt%, grain size was decreased by 80% while ultimate tensile strength and hardness were increased by 28% and 19% respectively in A357 alloys. Shi et al. [16] reported the addition of 0.3 wt% Er had the best effect on the refinement of α-Al grains and the morphology of eutectic Si phases.

Nogita et al. [17] investigated the eutectic Si modification efficiency of fourteen kinds of rare earth elements in Al–10Si alloy. It suggested that the structural transition was limited to a refinement of the coarse plate-like silicon structure to a finer, but still plate-like morphology, with exception of Eu. According to the previous study [18,19], it appears that the behavior of Eu is similar to that of Sr and Na. However, there is still a lack of detailed investigations on the optimum Eu concentration to obtain a fully fibrous eutectic Si. In particular, the effect of Eu on tensile properties of alloys has not been investigated in detail. Therefore, the aim of the present work is to investigate the effects of Eu addition and heat treatment on the microstructures and tensile properties of A356 alloys. Furthermore, fracture surfaces of as-cast and heat treated samples were also investigated.

2. Experimental details

A series of A356 alloys with different Eu contents (0, 0.02, 0.04, 0.06, 0.08, 0.1%, all percentages are in weight unless otherwise stated) were prepared by melting together commercial pure Al (99.7% purity), crystalline Si (99.3% purity), pure Mg (99.8% purity) and Al-6Eu master alloy at appropriate ratios. Firstly the pure Al ingot was charged into a resistance furnace to be adequately melted at 770 °C, and then appropriate Si was added into the Al melt and held for 30 min. When the temperature of melt decreased to 740 °C, pure Mg was added. Then preheated Al-6%Eu alloy was added into the melt, being stirred and held for 20 min to ensure homogeneous distribution of Eu. To eliminate gases and inclusions in the melts, the argon gas was injected into bottom of the furnace over 5 min by means of an iron pipe with a honeycomb end to generate small bubbles. The melt of 710 °C was poured into a metallic mould (92 mm × 90 mm × 30 mm) which was pre-heated to 200 °C. Table 1 presents the chemical composition and designation of alloys analyzed by X-ray fluorescence (XRF-1800). The ingots were cut along the longitudinal symmertric plane by an electric spark cutting method and then treated with a standard T6 schedule. The solution treatment was firstly performed at 540 °C for 12 h, and then quenched into water. The aging treatment was carried out at 155 °C for 8 h, and the samples were finally cooled in air.

Stainless steel crucibles coated with boron-nitride were used for thermal analysis and interrupted solidification (quenching) experiments. The crucibles were preheated at 750 °C for 20 min before interacting with the melt. Two parallel samples were simultaneously extracted by submerging the crucibles into the melt. The first crucible had a K type thermocouple in the center of the sample with the tip 25 mm from the bottom of the crucible. During solidification, the cooling curve form the thermocouple was monitored on a paperless recorder with a frequency of 100 Hz. The calibration of the thermocouple was checked before and after experimentation. The second crucible without the thermocouple was quenched by plunging the filled steel up in a water bath 40 s after the recalescence of the eutectic reaction had started.

Table 1
Chemical composition of the alloys (wt%).

Sample	Al	Si	Mg	Fe	Eu
Unmodified	Balance	6.9	2.9	0.17	0
0.02% Eu	Balance	7.3	3.1	0.18	0.012
0.04% Eu	Balance	7.2	2.8	0.18	0.028
0.06% Eu	Balance	7.4	2.8	0.16	0.069
0.08% Eu	Balance	6.9	3.0	0.16	0.079
0.1% Eu	Balance	7.1	2.9	0.16	0.095

The samples were grounded using SiC paper up to 1500 mesh. After a standard polishing procedure, these samples were then etched with a solution of 5 vol.% concentrated HF in 95 vol.% H_2O for microstructure examination. These samples were also deeply etched with a solution (15 vol.% HCl) to show the three-dimensional morphology of eutectic Si phase. The quenched samples were etched in a modified Murakami reagent (60 ml water, 10 g sodium hydroxide, 5 g potassium ferricyanide) for 60 s to better distinguish the solidified eutectic form quenched liquid. The samples were characterized by optical microscopy (OM, C2003A), scanning electron microscopy (SEM, Zeiss supra 55) equipped with facilities for energy dispersive spectroscopy (EDS) in secondary electron mode operated at 15 kV. The secondary dendrite arm spacing (SDAS), mean area and aspect ratio of eutectic Si phase were calculated with IPP 6.0 software. The measurement was done on 20 different areas of each microstructure in order to minimize the errors. To evaluate the effects of Eu and heat treatment on the mechanical properties of A356 alloys. The tensile specimens with a gauge length of 30 mm and a gauge diameter of 5 mm were cut from the alloys. The tensile strength was estimated using a computerized universal testing machine at room temperature at crosshead speed of 1.0 mm/min. The present values of tensile properties are calculated by the average of three tests for each alloy. The fracture surfaces of the failed tensile specimens were analyzed using SEM.

3. Results and discussion

3.1. Microstructure

Fig. 1 shows the optical microstructures of A356 alloys with different additions of Eu under as-cast condition, which demonstrate a substantial microstructural difference in the secondary dendrite arm spacing (SDAS) of α-Al and the size of eutectic Si. The SDAS of α-Al was quantitatively measured over 20 spatial fields in each specimen, as shown in Fig. 2. It is clear that the addition of Eu remarkably reduced the SDAS value. As 0.06% Eu was added to the A356 alloy, SDAS decreased from the unmodified 44 um to 34 um. While Eu content continued to increase, it remained relatively stable for increasing additions. The final secondary dendrite arm spacing (SDAS) of α-Al is determined by the process of dendrite arm coarsening. One kind of dendrite arm coarsening is that adjacent arms first coarsen and join at their middle part, then the coarsening dendrite extends from its middle to the root and head. The driving force for coalescence is due to the reduction of total solid–liquid interface area of the arms in the system [20]. Due to the low distribution coefficient of Eu element and low solid solubility in Al, excess of solute moves away from the solid–liquid interface. That is to say, the solute content and the width of the film among the dendrite arms increase with increasing Eu additions, which will hinder the coalescence of adjacent arms and refine the SDAS.

The high magnification 3D morphologies of eutectic Si in as-cast condition with different additions of Eu are depicted in Fig. 3. Figs. 1a and 3a show the clustered plate-like eutectic Si occurred in the unmodified alloy with an indistinct interface between α-Al and eutectic mixture. The introduction of Eu resulted in a better

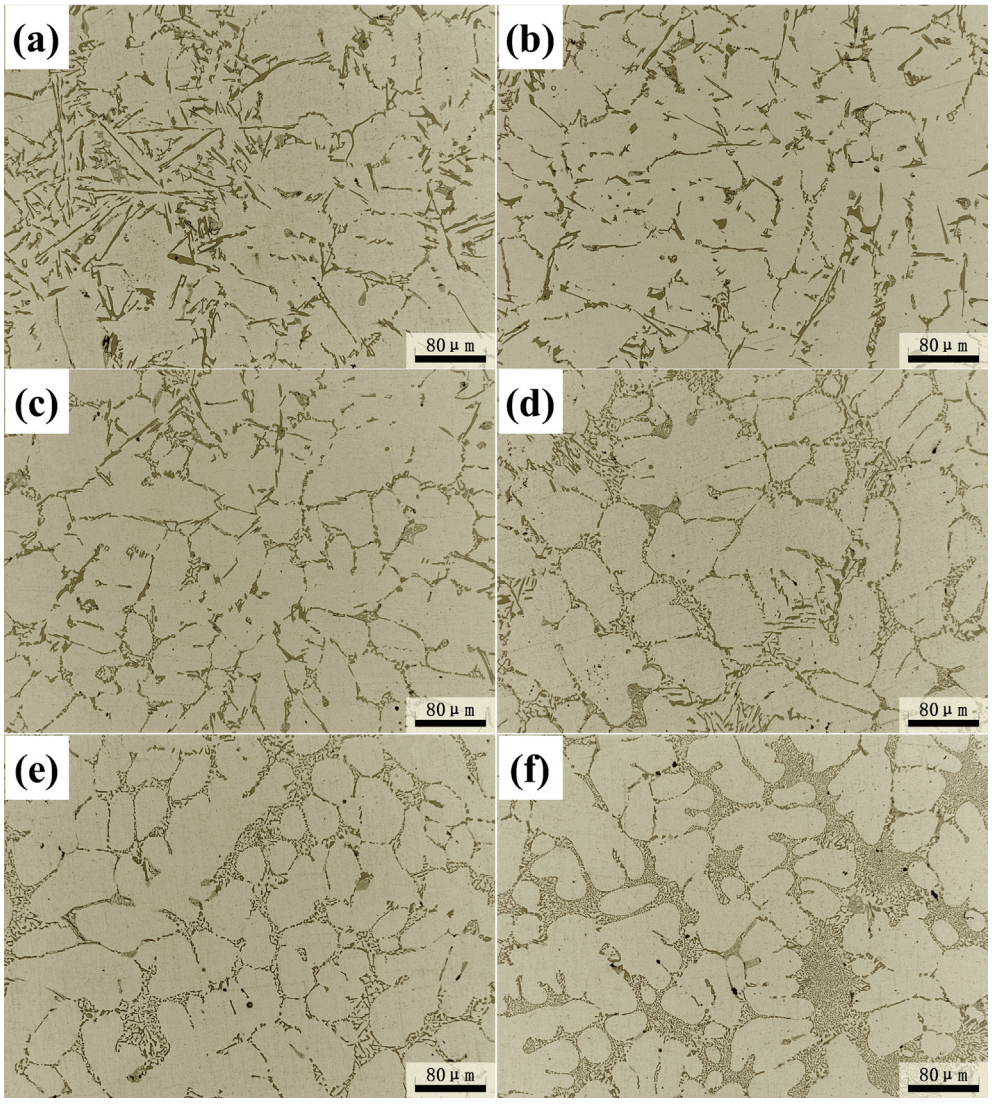

Fig. 1. The as-cast microstructures of A356 alloys: (a) unmodified, (b) 0.02 wt.% Eu, (c) 0.04wt.% Eu, (d) 0.06 wt.% Eu, (e) 0.08 wt.% Eu, (f) 0.1 wt.% Eu.

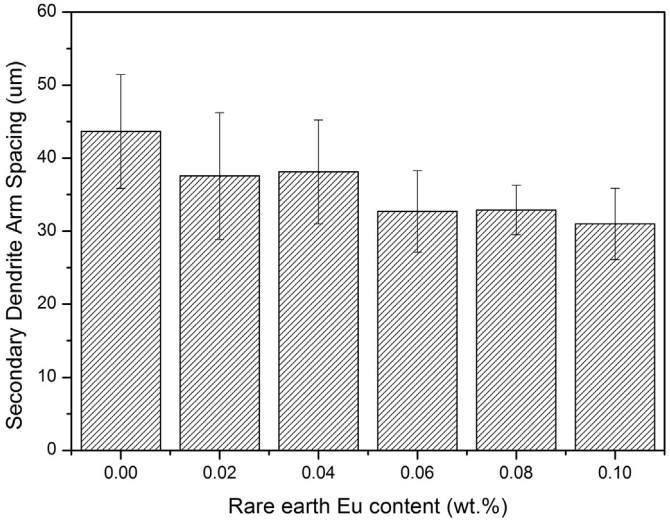

Fig. 2. Effect of Eu addition on SDAS.

distribution of eutectic Si with a smooth interface between α-Al and eutectic mixture, as shown in Fig. 1b–f. Figs. 1b and 3b indicate that there was no noticeable change in the size and morphology of eutectic Si with the introduction of 0.02% Eu. Further increased the Eu content to 0.08% resulted in the refinement of eutectic Si but the morphology was still the mixture of plate-like and branched structure, as shown in Fig. 3c–e. While from Figs. 1f and 3f, it can be seen that the 0.1% Eu modified alloy exhibited a fully modified, fine fibrous eutectic Si.

Fig. 4 presents the optical microstructures of A356 alloys with different additions of Eu after T6 heat treatment. It is clear that, the eutectic Si had spheroidized and coarsened to some extent after T6 treatment. Some eutectic Si particles in the unmodified alloy and 0.02% Eu modified alloy, however, still exhibited a longish rod-like morphology after heat treatment, as shown in Fig. 4a and b. Fig. 4c shows that the amount of longish rod-like eutectic Si decreased and the length of rod-like eutectic Si reduced simultaneously with the addition of 0.04% Eu. Further increasing the Eu content, a complete spheroidization of eutectic Si was observed, as shown in Fig. 4d–f. The difference of fragmentation and spheroidization of eutectic Si could be attributed to the modification rating [14].

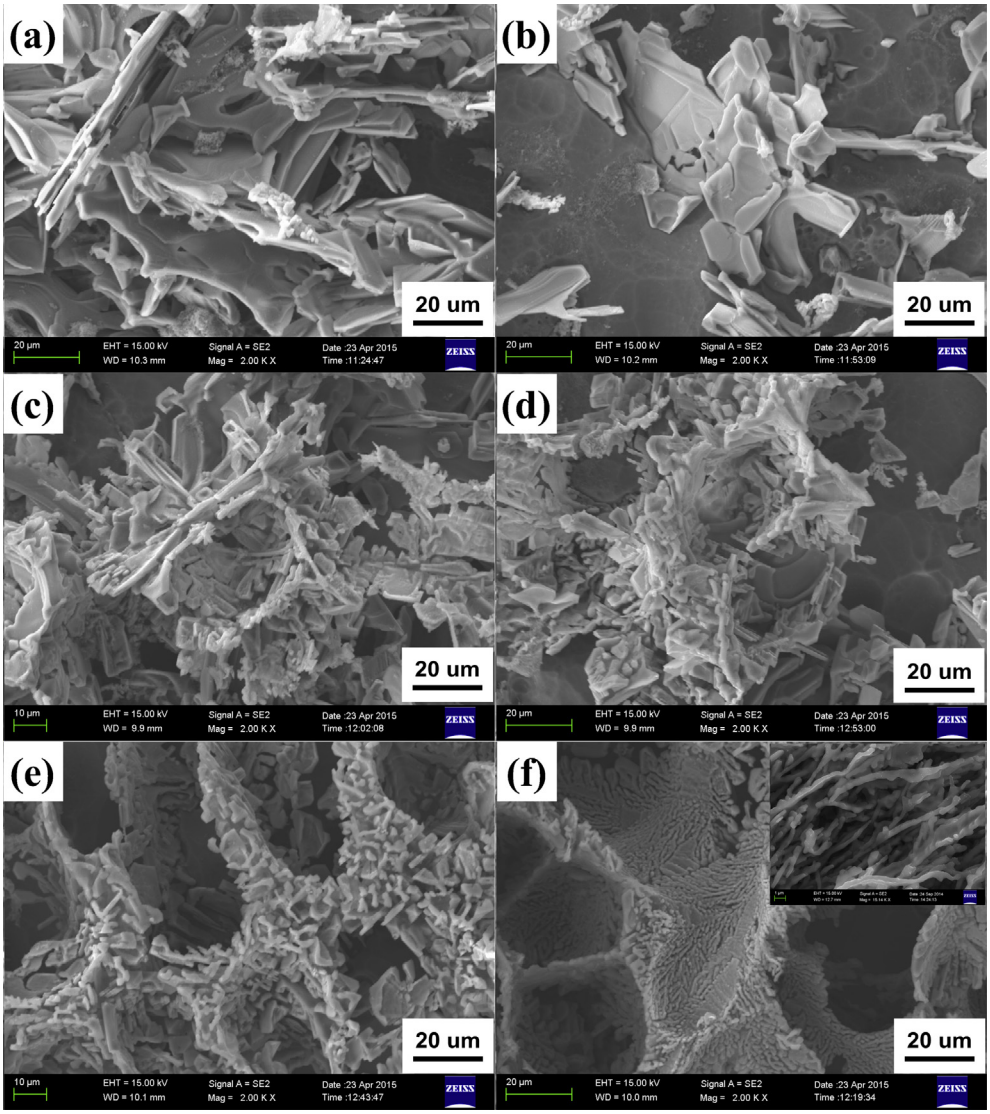

Fig. 3. High magnification three-dimensional morphology of eutectic Si in A356 alloys: (a) unmodified, (b) 0.02 wt.% Eu, (c) 0.04wt.% Eu, (d) 0.06 wt.% Eu, (e) 0.08 wt.% Eu, (f) 0.1 wt.% Eu.

Two geometric parameters, mean area and aspect ratio, are selected to characterize the eutectic Si of A356 alloys under as-cast and T6 heat treatment conditions, as shown in Fig. 5. According to the results obtained from the geometric parameters in Fig. 5, it is clear that the mean area and aspect ratio of eutectic Si decreased with increasing Eu content under as-cast condition. The trend in Fig. 5 demonstrates that an optimum Eu addition level under as-cast condition was 0.1%. The heat treated alloys had a higher mean area and a lower aspect ratio of eutectic Si due to the coarsening and spheroidization of eutectic Si after T6 treatment. Both the mean area and aspect ratio of the T6-tempered had identical trend with that of the as-cast alloys. Note that there was no noticeable difference in the mean area and aspect ratio of eutectic Si between the Alloy E (Fig. 5e) and the Alloy F (Fig. 5f), though great different morphologies of eutectic Si existed in as-cast condition (Fig. 4e and f). Correlating with the as-cast samples, the 0.1% Eu modified A356 alloy achieved likewise full modification of eutectic Si particles with lowest mean area and aspect ratio.

At low Eu contents, few Eu-rich intermetallics were observed in the microstructure. But when the content of Eu increased up to 0.1%, some Eu-rich intermetallics were clearly observed in the microstructure. Fig. 6a and 6b show the secondary electron image and back scattered electron image (BSE) of the 0.1%Eu modified alloy respectively. The Eu-rich intermetallics are brighter in BSE image because of the bigger atomic number of Eu element. The coarse and small Eu-rich intermetallics were both found in Al matrix, as shown in Fig. 6b. Fig. 6c is an enlarged area marked (C) with a red box in Fig. 6b, showing some small Eu-rich particles (less than 1 um) in eutectic mixture. Fig. 6e is an enlarged area marked (E) with a red circle, showing two coarse Eu-containing particles (more than 2 um) with an irregular polygonal morphology. The results of EDS analysis show that the compositions of two Eu-rich particles were different, as shown in Fig. 6g and h. However, a lot of repetitive EDS analysis on more Eu-containing compounds show that most of the coarse Eu-rich intermetallics were Al_2Si_2Eu (Fig. 6h) according to the atomic percentages, which was very similar to the Al_2Si_2Yb phase observed in the Al–Si-Yb based alloy [21]. The small Eu-rich particles can be seen more clearly in Fig. 7 at a higher magnification, which were observed within eutectic Si or on the edge of eutectic Si. This is in agreement with the investigation carried out by Li et al. [19]. He pointed Eu that has not been

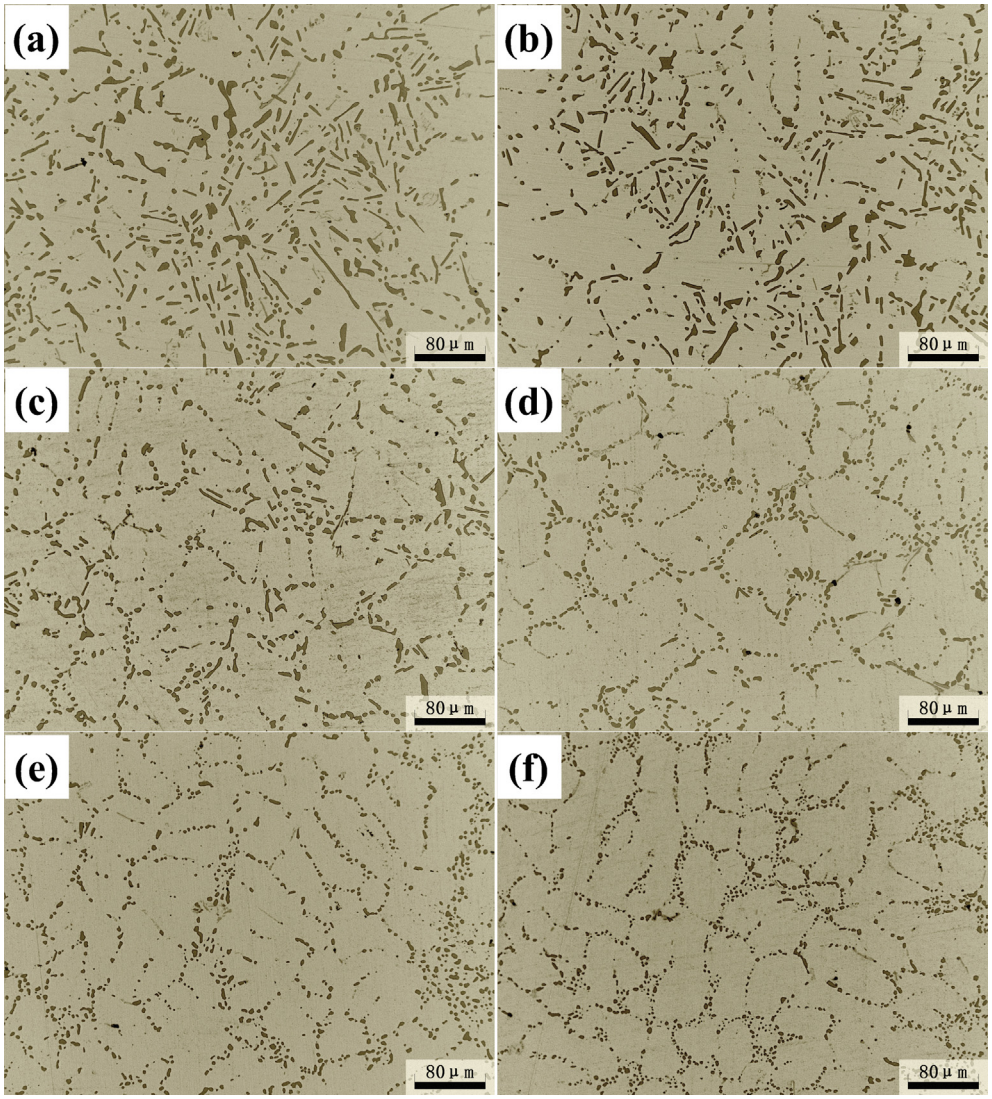

Fig. 4. The heat treated microstructures of A356 alloys: (a) unmodified, (b) 0.02 wt.% Eu, (c) 0.04wt.% Eu, (d) 0.06 wt.% Eu, (e) 0.08 wt.% Eu, (f) 0.1 wt.% Eu.

adsorbed within eutectic Si will be segregated out of the Si during eutectic Si growth at high Eu contents and the small Eu-rich particles were most likely to be Al_2Si_2Eu. It should be noted that these coarse Eu-rich particles can be clearly distinguished by EDS mapping, but these small coarse Eu-rich particles cannot because of its limited resolution, as shown in Fig. 6d and f.

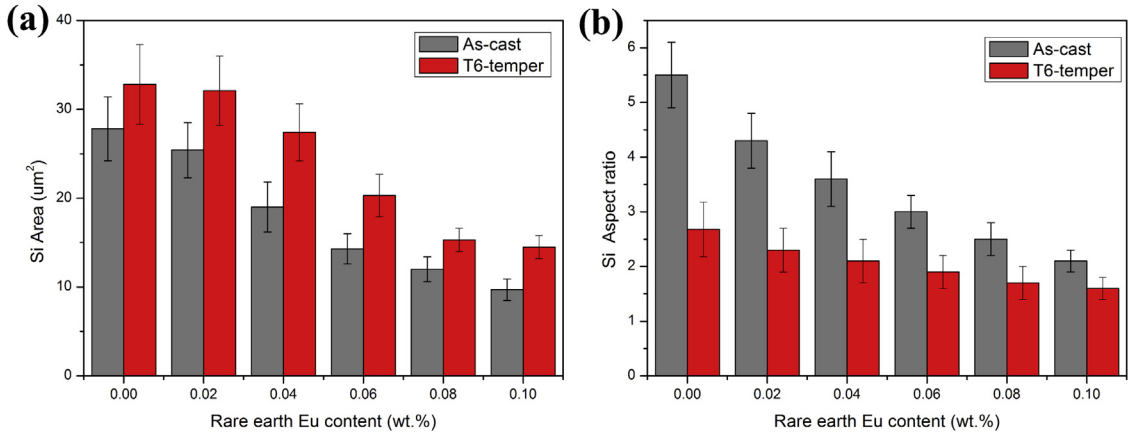

Fig. 5. Effect of Eu addition on geometric parameters of eutectic Si in A356 alloys: (a) mean area, (b) aspect ratio.

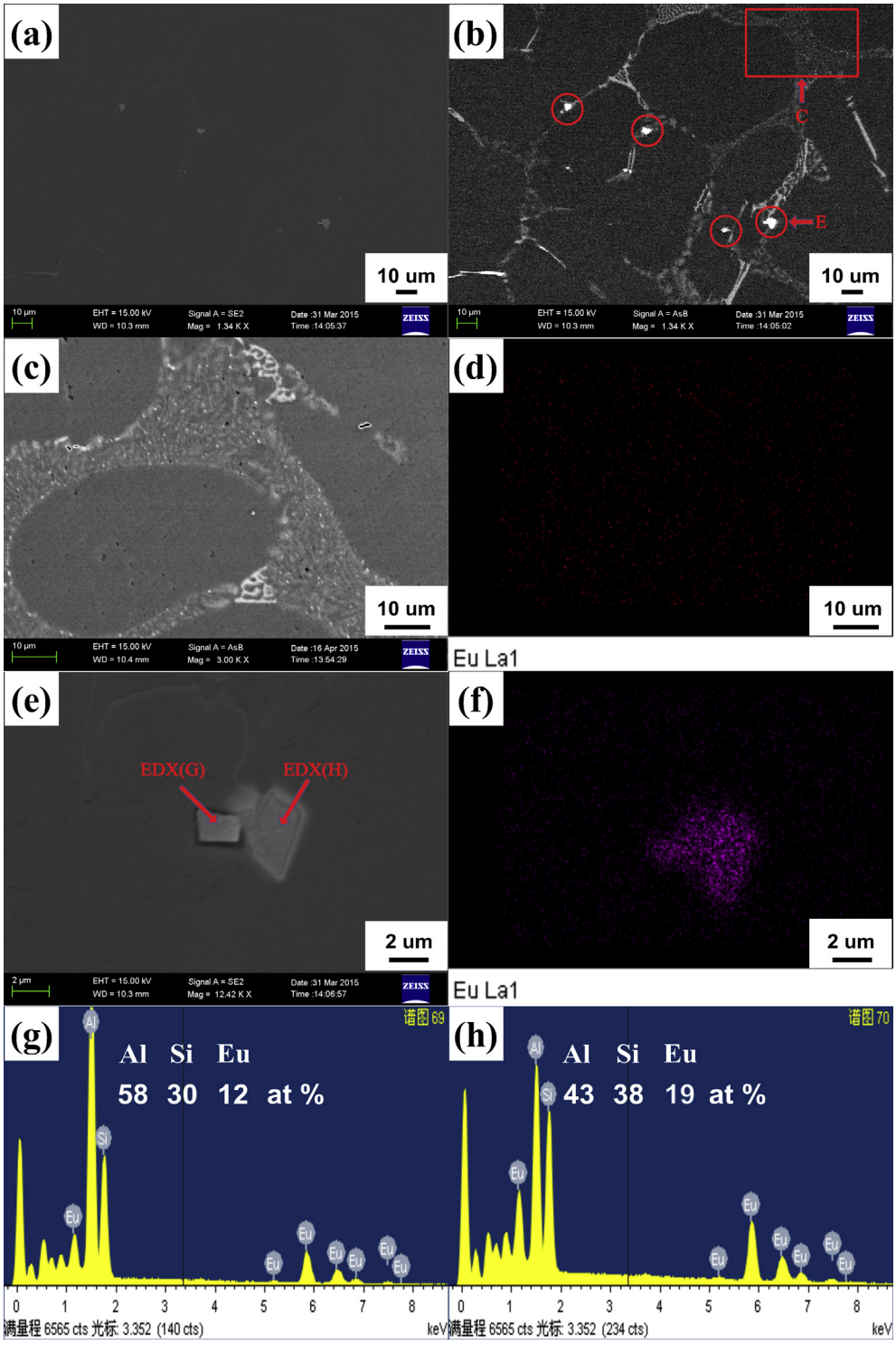

Fig. 6. (a) Secondary electron image, (b) back scattered electron image in the 0.1wt.%Eu modified alloy, (c) is enlarged from the area marked with a red box C in (b), (d) Eu element distribution in (c), (e) is enlarged from the area marked with a red circle E in (b), (f) Eu element distribution in (e), (g) EDX analysis of particles marked with EDX(G) in (e), (h) EDX analysis of particles marked EDX(H) in (e). (For interpretation of the references to colour in this figure legend, the reader is referred to the web version of this article.)

3.2. Thermal analysis

Fig. 8a shows an assembly of cooling curves taken form A356 alloys with and without Eu addition. The liquidus temperature of the unmodified A356 alloy (Alloy A) was evaluated to be about 615 °C, as shown in Fig. 8b. It can be clearly observed that the solidification behavior of primary α-Al was not significantly changed with the addition of Eu. The eutectic arrest area is enlarged, as shown in Fig. 8c. The eutectic nucleation temperature (T_N), minimum temperature (T_{Min}), and growth temperature (T_G) are listed in Table 2 by calculating their derivatives [21]. The measured T_N of eutectic Si (572 °C) was close to the equilibrium

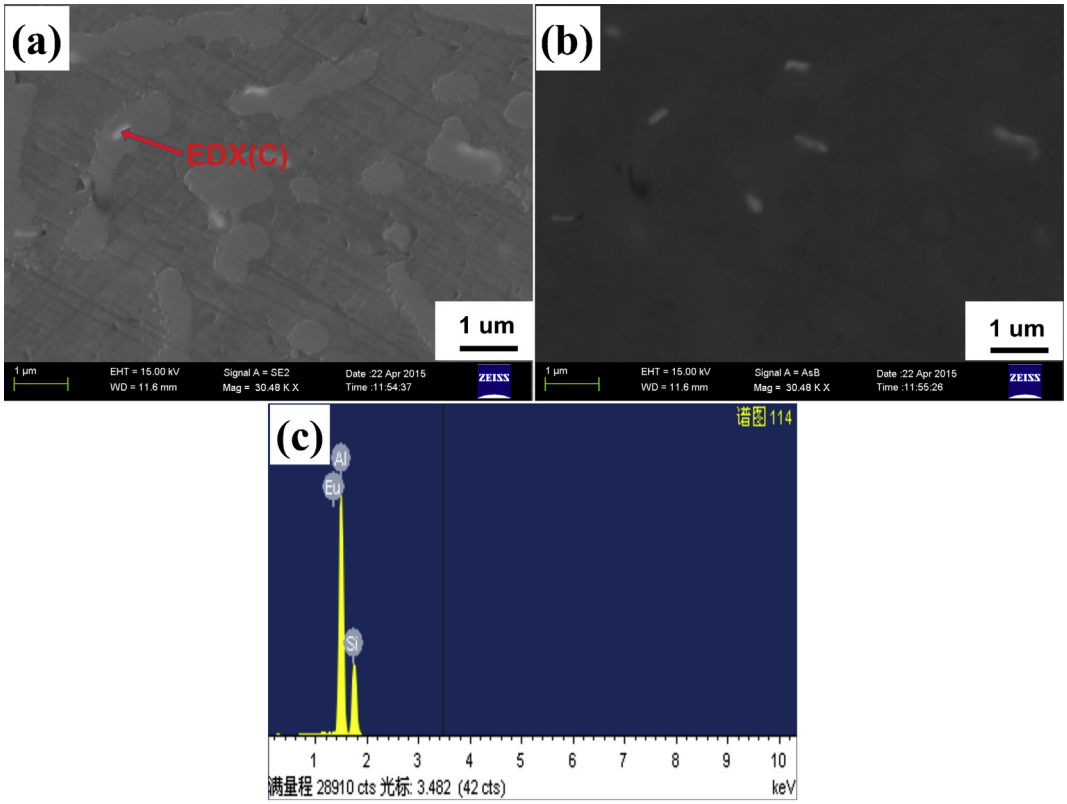

Fig. 7. (a) Secondary electron image, (b) back scattered electron image of small Eu-rich particles in the 0.1wt.%Eu modified alloy, (c) EDX analysis of particles marked EDX(C) in (a).

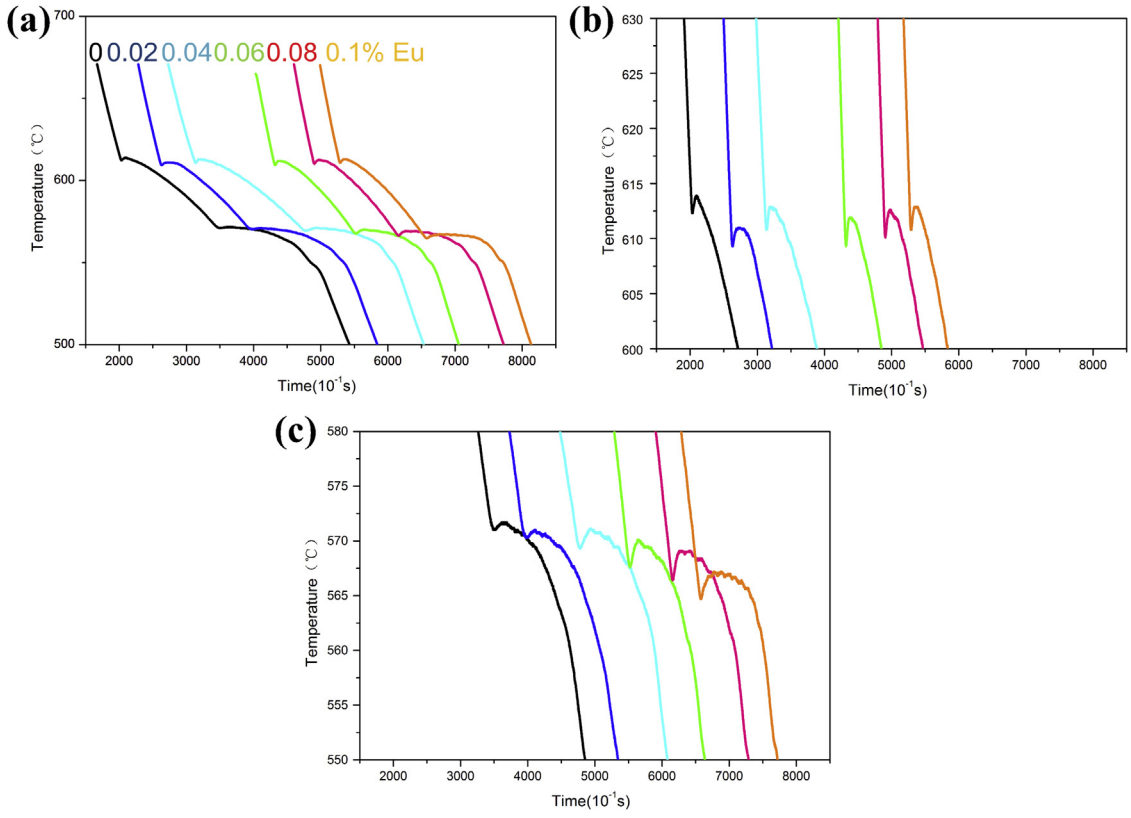

Fig. 8. Cooling curves (a) taken from A356 alloys with and without Eu addition. The nucleation of α-Al is enlarged in (b). The eutectic arrest area is enlarged in (c).

Table 2
Nucleation temperature (T_N), Minimum temperature (T_{Min}), Growth temperature (T_G), Nucleation undercooling ($T_{eq} - T_N$), Growth undercooling ($T_{eq} - T_G$), and Recalescence ($T_G - T_{Min}$) for A356 alloys with and without Eu addition.

Alloys	T_N (°C)	T_{Min} (°C)	T_G (°C)	Nucleation undercooling $T_{eq} - T_N$ (°C)	Growth undercooling $T_{eq} - T_G$ (°C)	Recalescence $T_G - T_{Min}$ (°C)
A	572.0	571.0	571.7	2.0	2.3	0.7
B	570.7	570.3	571.0	3.3	3.0	0.7
C	570.0	569.3	571.1	4.0	2.9	1.8
D	569.1	567.6	570.0	4.9	4.0	2.4
E	567.5	566.5	569.0	6.5	5	2.5
F	566.1	564.7	567.2	7.9	6.8	2.5

eutectic temperature Teq (574 °C) predicted by Li et al. [21] in commercial purity condition. With increasing Eu addition, the eutectic nucleation temperature (T_N), minimum temperature (T_{Min}), and growth temperature (T_G) were displaced to lower temperatures.

The nucleation undercooling (Teq − T_N), grow undercooling (Teq − T_G) and recalescence ($T_G - T_{Min}$) of the eutectic arrest is also determined. No significant nucleation undercooling (2 °C) and grow undercooling (2.3 °C) were observed in the unmodified alloy. Increasing Eu addition resulted in increasing nucleation undercooling (i.e., 6.5 °C in the 0.08%Eu modified alloy and 7.9 °C in the 0.1%Eu modified alloy) and increasing growth undercooling (i.e., 5 °C in the 0.08%Eu modified alloy and 6.8 °C in the 0.1%Eu modified alloy). However, the recalescence ($T_G - T_{Min}$) increased by the initial addition of Eu, while it remained relatively stable for increasing additions (above 0.06%). In addition, the nucleation undercooling (Teq − T_N) and growth undercooling (Teq − T_G) of the eutectic arrest show a good prediction to the modification of eutectic Si, but no direct relationship can be expected between the Si morphology and the recalescence of eutectic arrest.

3.3. Quenching analysis

Fig. 9 shows the typical micrographs of the quenched samples 40 s after the recalescence of the eutectic reaction. The unmodified, 0.06%Eu and 0.1%Eu modified samples are chosen for characterization in the quenching experiment. Fig. 9a indicates that a large number of eutectic grains were present in the unmodified alloy. However, the number of eutectic grains decreased with increasing Eu content, as shown in Fig. 9c and e. In particularly, very few eutectic grains were observed in the 0.1%Eu modified alloys. The high magnification micrographs of the quenched unmodified and 0.06%Eu modified alloys show the eutectic grains were located at or close to the tips of the aluminum dendrites with a jagged solid–liquid interface, as shown in Fig. 9b and d. In contrast, the eutectic grains were formed in the interdendritic region with a smooth solid–liquid interface in 0.1% Eu modified alloy, as shown in Fig. 9f.

3.4. Mechanism of modification on eutectic Si

There are two extensively studied mechanisms causing the significant change in eutectic silicon: restricted nucleation theory [22–24] and restricted growth theory [18,25,26]. The restricted nucleation mechanisms concentrate on nucleation alterations caused by the modifier. The increased nucleation undercooling (Teq − T_N) and few eutectic grains suggest that the addition of Eu may influence the nucleation kinetics in such way by eliminating some heterogeneous sites in the liquid, such as Fe-containing intermetallic phase [24], AlP phase [27–32] and oxide bi-films [33,34]. The location of eutectic grains locating at or close to the tips of the aluminum dendrites indicates that the nuclei are pushed ahead of dendrite–liquid interface during solidification. In Eu-containing alloys, the nuclei would not play a significant role in the nucleation of the eutectic grains and far fewer eutectic grains form in the interdendritic liquid [25,32]. Thereby, the reduced nucleation density is proposed to cause an increase in the growth rate because of the smaller solid–liquid interface area and modify the eutectic Si [35].

The restricted growth theory focuses on the effect of Eu on the growth of eutectic Si phase. Li et al. [19] found that the formation of Eu-rich clusters within eutectic Si were observed along the $<112>_{Si}$ growth direction of Si and at the intersection of two $\{111\}_{Si}$ twins, providing strong experimental support for IIT (impurity induced twinning) and poisoning of TPRE (twin plane re-entrant edge) growth mechanisms. With regard to the IIT mechanism, a value of 1.65 was proposed as the ideal value for the ratio of atomic radius of modifier to that of silicon [36]. Eu has an atomic ratio of r/r_{si} (1.75) close to the ideal value. Despite all this, it should be noted that either the poisoning of TPRE mechanism or ITT mechanism can be attributed to the interfacial poisoning of Si at the growing interface, highlighting the importance of the absorption of modifier atoms to the growing interface. Recently the results of u-XRF (X-ray fluorescence) and XAFS (X-ray absorption fine structure) showed that Eu element had a strong bonding with Si [18,19].

3.5. Tensile properties

Table 3 presents the tensile properties including tensile strength and elongation of A356 alloys with different additions of Eu under as-cast and T6 conditions. It is confirmed that mechanical properties of the Al–Si casting alloys are known to be largely dependent on the size, morphology and distribution of eutectic Si [37]. Table 3 indicates that the maximum improvement of UTS values in both ac-cast and T6 conditions (about 15.9% in as-cast alloy and 6% in T6 heat treated alloy) were obtained from the 0.1% Eu modified alloy with a fully modified structure, though the ultimate tensile strengths did not show significant difference with different levels of Eu after T6 treatment. The maximum improvement of EI values in both ac-cast and T6 conditions (about 24.3% in as-cast alloy and 54.1% in T6 heat treated alloy) were obtained from the 0.08% Eu modified alloy. However, the EI value decreased with increasing Eu content to 0.1% in both ac-cast and T6 conditions. The coarse Al_2Si_2Eu particles may cause high levels of stress concentration and consequently have a deleterious effect on it.

To evaluate the tensile test date, a quality index, which is defined as $Q = UTS + a \times \log(\text{elongation})$ was calculated, where a is 150 for Al–Si–Mg alloys [38]. This concept arose from the consideration of the relationship between ultimate tensile strength and elongation of Al–Si–Mg alloys. Since the quality index combines both strength and ductility, it is much more descriptive of the true tensile properties of a casting than either the tensile strength or the elongation alone [39]. According to the results of quality index (Q), the maximum improvement of Q values in both as-cast and T6 conditions (about 11.4% in as-cast alloy and 10.8% in T6 heat treated alloy) were obtained from the 0.1% Eu modified alloy. An optimal

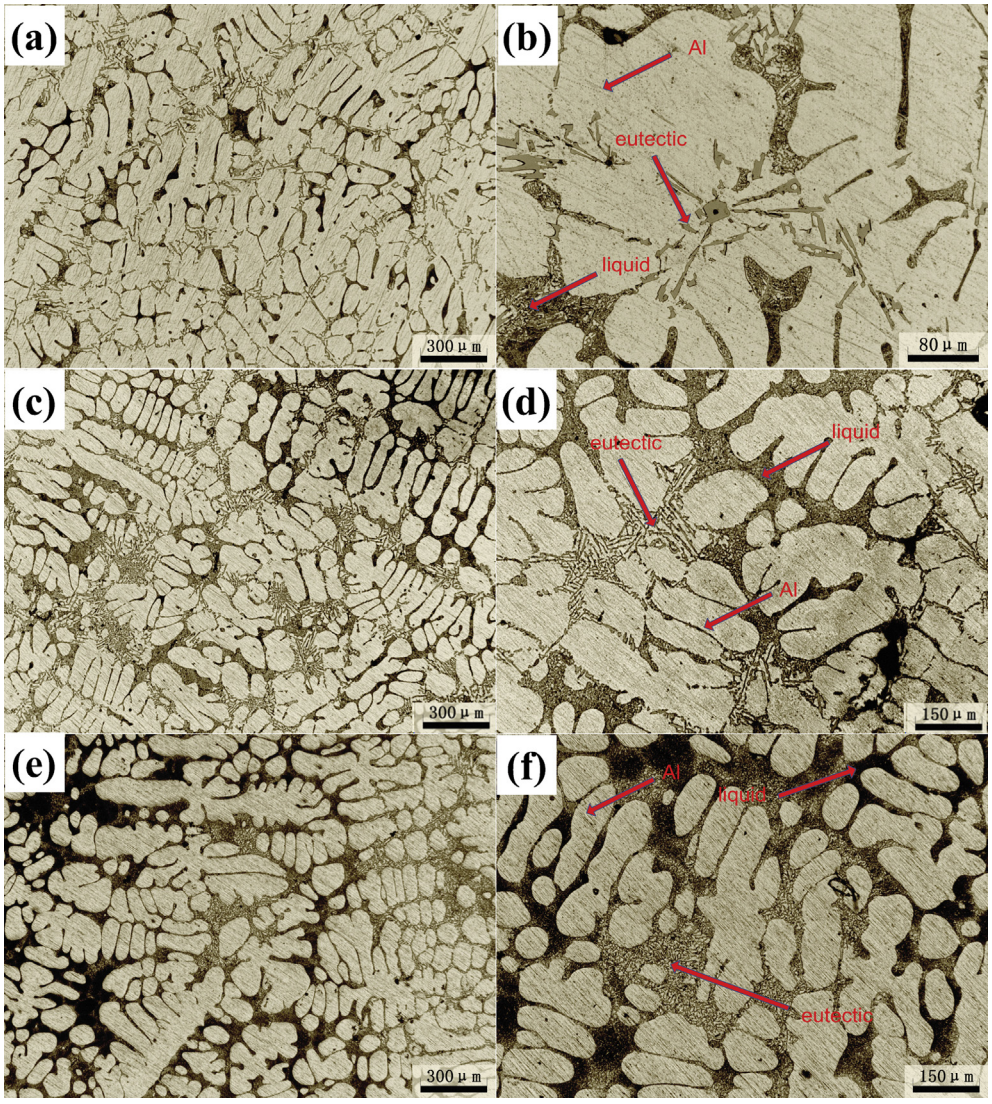

Fig. 9. The microstructures of quenched A356 alloys: (a and b) unmodified, (c and d), 0.06wt.% Eu, (e and f) 0.1wt.% Eu.

combination of UTS (265 MPa) and EI (14.7%) of A356 alloy was achieved by the 0.1% Eu addition combined with T6 heat treatment.

3.6. Fractography

Fig. 10 presents the fracture surfaces of A356 alloys with different additions of Eu under as-cast and T6 heat treatment conditions. It can be clearly seen that extensive irregular planes were apparent on the entire fracture surface of the unmodified alloy as shown in Fig. 10a, showing a clear brittle fracture nature. Fig. 10b indicates that the introduction of 0.04% Eu decreased the area of the cleavage planes and increased the number of dimples due to the refinement of eutectic Si. Moreover, the modification efficiency enhanced with the further increase of Eu content in the alloy. As a result, the fracture surfaces of 0.06%Eu and 0.1%Eu modified alloys were covered mainly by dimples, indicating a ductile fracture phenomena leading to a higher tensile elongation, as shown in Fig. 10c and d. T6 heat treatment further enhanced the strength and elongation of A356 alloys significantly. Therefore, many dimples and some tearing ridges were clearly found on the fractures surfaces, indicating a much more ductile failure mode compared with the ac-cast alloys. Fig. 10f shows that few dimples were distributed unevenly in the fracture surfaces of the A356 unmodified alloy after T6 treatment with the size ranging from 5 um to 30 um, due to the partial fragmentation and spheroidization of eutectic Si. The dimples became smaller and more uniform with increasing Eu addition, as shown in Fig. 10f–h. Especially the fracture surface of the T6 heat treated 0.1%Eu modified alloy exhibited an obvious ductile fracture with the size of the dimples

Table 3
Tensile properties of alloys for various specimens.

	Alloy	Tensile strength (MPa)	Elongation (%)	Quality index (MPa)
As-cast	A	176 ± 22.1	7.4 ± 1.3	306
	B	174 ± 17.5	7.3 ± 1.2	303
	C	187 ± 8.1	7.7 ± 2.8	319
	D	188 ± 10	8.9 ± 3.0	330
	E	190 ± 3.7	9.2 ± 0.6	334
	F	204 ± 27.5	8.2 ± 3.3	341
T6	A	250 ± 13.2	9.6 ± 3.1	397
	B	252 ± 12.6	9.8 ± 2.6	400
	C	262 ± 2.8	12.8 ± 4.1	428
	D	263 ± 7.6	13.7 ± 5.1	433
	E	261 ± 5.7	14.8 ± 1.4	436
	F	265 ± 5.0	14.7 ± 5.6	440

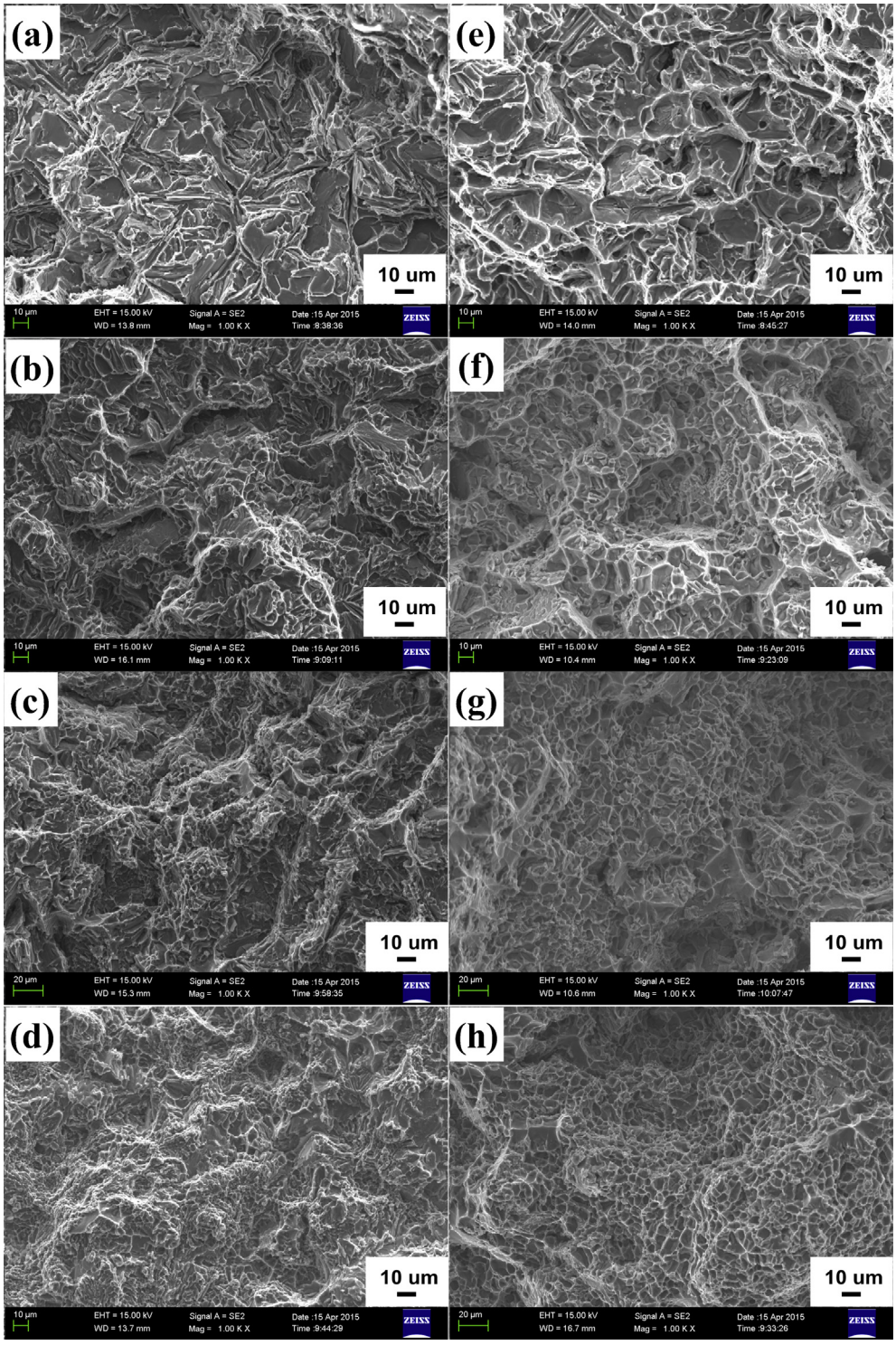

Fig. 10. Fractographs of A356 alloys with various content of Eu; (a and e) unmodified, (b and f), 0.04wt.% Eu, (c and g) 0.06wt.% Eu, (d and h) 0.1wt.% Eu, (a–d) as-cast condition and (e–h) T6 heat treatment condition.

distributing more uniformly ranging from 3 um to 6 um, as shown in Fig. 10h. The existence of deep and fine dimples in Fig. 10h shows the higher ductility of the modified alloys. As a whole, the findings from the fractographs are in good agreement with the variations in fracture modes and ductility of different samples (Table 3).

4. Conclusions

The effect of Eu on the microstructures and mechanical properties of A356 aluminum alloys was studied. The following conclusions were drawn:

(1) The addition of Eu remarkably reduced the size of eutectic Si as well as the SDAS value of primary α-Al. The refinement efficiency enhanced with the increase of Eu content in the alloy. The addition of 0.1%Eu modified the eutectic Si from a coarse plate-like form to a fully modified and fine fibrous one.
(2) T6 treatment encouraged the spheroidization of eutectic Si particles. Correlating with the as-cast samples, the 0.1%Eu modified A356 alloy achieved likewise full modification of eutectic Si particles with lowest mean area and aspect ratio.
(3) When the content of Eu increased up to 0.1%, the coarse and small Eu-rich intermetallics were both observed in Al matrix. Most of the coarse Eu-rich intermetallics phases (more than 2 um) were Al_2Si_2Eu and the small Eu-rich intermetallics (less than 1 um) were observed within eutectic Si or on the edge of eutectic Si.
(4) With increasing Eu addition, the eutectic nucleation temperature (T_N), minimum temperature (T_{Min}), and growth temperature (T_G) were displaced to lower temperatures. Increasing Eu addition resulted in increasing nucleation undercooling and increasing growth undercooling. However, the recalescence ($T_G - T_{Min}$) increased by the initial addition of Eu, while it remained relatively stable for increasing additions (above 0.06%).
(5) A large number of eutectic grains were located at or close to the tips of the aluminum dendrites with a jagged solid−liquid interface in unmodified alloy, while very few eutectic grains were formed in the interdendritic region with a smooth solid−liquid interface in 0.1%Eu modified alloy.
(6) The transition from brittle to ductile fracture mode after modification was accompanied by an increase in the UTS and EI of the as-cast alloys. T6 heat treatment further enhanced the strength and elongation of A356 alloys significantly. Few dimples were distributed unevenly in the fracture surfaces of the unmodified alloy after T6 treatment with the size ranging from 5 um to 30 um. In contrast, 0.1%Eu modified alloy exhibited an obvious ductile fracture with the size of the dimples distributing more uniformly ranging from 3 um to 6 um. An optimal combination of UTS (265 MPa) and EI (14.7%) of A356 alloy was achieved by the 0.1%Eu addition combined with T6 heat treatment.

Acknowledgments

The authors thank the National Natural Science Foundation of China (Nos.51071035, 51375070, 51274054, U1332115), and the Key grant Project of Chinese Ministry of Education (No.313011).

References

[1] O.E.I. Sebaie, A.M. Samuel, F.H. Samuel, H.W. Doty, Mater. Sci. Eng. A 456 (2008) 241–252.
[2] M. Faraji, L. Katgerman, Micron 41 (2010) 554–559.
[3] M. Tiryakioğlu, Mater. Sci. Eng. A 427 (2006) 154–159.
[4] D.L. Zhang, L.H. Zheng, D.H. Stjohn, J. Light Met. 2 (2002) 263–269.
[5] M. Zarif, B. Mckay, P. Schumacher, Metall. Mater. Trans. A 42A (2011) 1684–1691.
[6] X. Jian, T.T. Meek, Q. Han, Scr. Mater. 64 (2006) 893–896.
[7] J.B. Yu, Z.M. Ren, K. Deng, Acta. Metall. Sin. 24 (2011) 301–308.
[8] M. Timpel, N. Wanderka, R. Schlesiger, Acta Mater. 60 (2012) 3920–3928.
[9] J.H. Li, J. Barrirero, M. Engstler, H. Aboulfadl, F. Mucklich, P. Schumacher, Metall. Mater. Trans. A 46 (2015) 1300–1311.
[10] S. Farahany, M.H. Idris, A. Ourdjini, Thermochim. Acta 584 (2014) 72–78.
[11] Y.C. Tsai, C.Y. Chou, S.L. Lee, C.K. Lin, J.C. Lin, S.W. Lim, J. Alloys Compd. 487 (2009) 157–162.
[12] Y.C. Tsai, S.L. Lee, C.K. Lin, J. Chin. Inst. Eng. 34 (2011) 609–611.
[13] H.X. Qiu, H. Yan, Z. Hu, J. Alloys Compd. 567 (2013) 77–81.
[14] B. Li, H.W. Wang, J.J. Jin, Z.J. Wei, Mater. Des. 32 (2011) 1617–1622.
[15] M. Arfan, X. Cong, X.J. Wang, H. Shuji, Y. Hiroshi, R.H. Li, C.L. Ma, Mater. Sci. Eng. A 604 (2014) 122–126.
[16] Z.M. Shi, Q. Wang, G. Zhao, R.Y. Zhang, Mater. Sci. Eng. A 626 (2015) 102–107.
[17] K. Nogita, S.D. Mcdonald, A.K. Dahle, Mater. Trans. 45 (2004) 323–326.
[18] K. Nogita, H. Yasuda, M. Yoshiya, S.D. Mcdonald, K. Uesugi, A. Takeuchi, et al., J. Alloys Compd. 489 (2010) 415–420.
[19] J.H. Li, X.D. Wang, T.H. Ludwing, Y. Tsunekawa, L. Arnberg, J.Z. Jiang, et al., Acta Mater. 84 (2015) 153–163.
[20] G.D. Gu, G.Y. An, Foundry 10 (1990) 32–35.
[21] J.H. Li, S. Suetsugu, Y. Tsunekawa, P. Schumacher, Metall. Mater. Trans. A 44A (2013) 669–681.
[22] P. Srirangam, M. Kramer, S. Shankar, Acta Mater. 59 (2011) 503–513.
[23] M.M. Makhlouf, H.V. Guthy, J. Light Met. 1 (2001) 199–218.
[24] S. Shankar, Y. Riddle, M.M. Makhlouf, Acta Mater. 52 (2004) 4447–4460.
[25] S.D. McDonald, K. Nogita, A.K. Dahle, Acta Mater. 52 (2004) 4273–4280.
[26] K. Nogita, H. Yasuda, K. Yoshida, K. Uesugi, A. Takeuchi, Y. Suzuki, et al., Scr. Mater. 55 (2006) 787–790.
[27] K. Nogita, S.D. McDonald, K. Tsujimoto, K. Yasuda, A.K. Dahle, J. Electron Microsc. 53 (2004) 361–369.
[28] C.R. Ho, B. Cantor, J. Mater. Sci. 30 (1995) 1912–1920.
[29] P.B. Crosley, L.F. Mondolfo, AFS Trans. 74 (1966) 53–64.
[30] C.R. Ho, B. Cantor, Acta Metall. Mater. 43 (1995) 3231–3324.
[31] J.H. Li, M.Z. Zarif, M. Albu, B.J. McKay, F. Hofer, P. Schumacher, Acta Mater. 72 (2014) 80.
[32] Y.H. Cho, H.C. Lee, K.H. Oh, A.K. Dahle, Metall. Mater. Trans. A 39 (2008) 2435–2448.
[33] J. Campbell (Ed.), Complete Casting Handbook, Elsevier, Oxford, 2011, pp. 279–334.
[34] G. Sigworth, Int. J. Met. Cast. 2 (2008) 19–22.
[35] S.D. McDonald, A.K. Dahle, J.A. Taylor, D.H. Stjohn, Metall. Mater. Trans. A 35A (2004) 1829–1837.
[36] S.Z. Lu, A. Hellawell, Metal. Mater. Trans. A 18 (1987) 1721–1733.
[37] T. Kobayashi, Mater. Sci. Eng. A 280 (2000) 8–16.
[38] M. Drouzy, S. Jacob, M. Richard, AFS Int. Cast. Met. J. 5 (1980) 43–50.
[39] G.S. Mousavi, M. Emamy, J. Rassizadehghani, Mater. Sci. Eng. A 556 (2012) 573–581.